Stochastic Environmental Research and Risk Assessment (2022) 36:2285–2301
https://doi.org/10.1007/s00477-021-02112-y

ORIGINAL PAPER

Analysis of precipitation dynamics at different timescales based on entropy theory: an application to the State of Ceará, Brazil

Larissa Zaira Rafael Rolim[1] · Samiria Maria Oliveira da Silva[1] · Francisco de Assis de Souza Filho[1]

Accepted: 4 October 2021 / Published online: 6 November 2021

Abstract
Water resource variables are highly complex and vary both spatially and temporally. Understanding the variability and how it evolves has been an important scientific question in Ceará, Brazil. However, describing and determining the uncertainty and the variability in precipitation is still a challenge. Assessing the uncertainty around precipitation is key to develop robust and proactive planning. This study's main aim is to evaluate the underlying spatiotemporal variability of precipitation in the State of Ceará at different timescales by using standardized variability indices computed from different entropy measures. This methodology was applied to analyze 31 meteorological stations with daily time series from 1962 through 2006 while expanding the analysis to the remaining region using an interpolation method. The seasonal timescale analysis revealed that the dry season contributes more to the annual variability, and the change in intra-annual precipitation dynamics could vary with timescales. There were significant upward trends in entropy. Thus, for some stations, there was an increase in the uncertainty of rainfall. Also, there was an increase in variability amount and intensity throughout the decades at the monthly and seasonal timescales. Assessment of precipitation uncertainty within different timescales can benefit a broad community of scientists who are interested in arid-region and natural hazards.

Keywords Complexity · Entropy · Rainfall · Spatiotemporal variability · Trend analysis · And Uncertainty

1 Introduction

Arid and semi-arid regions are characterized by hydrological constraints such as rising temperatures, low annual mean precipitation, frequent droughts, and inter-annual to higher-scales variations, making these areas vulnerable to climate variability (Ramarao et al. 2019; Singh and Chudasama 2021). Changes in the hydrological cycle caused by climate variability and change have severe impacts on the amount and distribution of hydrological variables, leading to water availability and water quality changes (Jemai et al. 2017; Zheng et al. 2017).

The State of Ceará is located in the Northeastern region of Brazil (NEB), the most densely populated semi-arid region of the planet. The NEB has been reported as one of the world's most vulnerable areas to climate change in the coming century (IPCC 2014). Future climate projections in NEB show significant temperature increases, and rainfall reductions caused by climate change and human activities (Wu et al., 2016; Marengo et al. 2017; De Jong et al. 2018). Hydrological variability analysis in drought-prone environments plays a critical role in water resources planning and management (Cirilo et al. 2017). Thus, in response to the increased risk of extreme events, climate risk assessment has an essential role in climate adaptation. However, the task of understanding the spatiotemporal complexity of hydrological variables remains a great challenge (Mishra and Singh 2010; Tongal and Sivakumar 2019; Guntu et al. 2020).

Precipitation is an important meteorological parameter for comprehending hydrological extremes. Complex changes in climate and hydrological systems can be indicated through rainfall patterns and trends, making it an essential assessment for efficient and sustainable water resources management. The uncertainty linked to precipitation variation poses a major obstacle to regional water resources and socio-economic development (Jemai et al.

✉ Larissa Zaira Rafael Rolim
larissazairarr@gmail.com

[1] Dept. of Hydraulic and Environmental Engineering, Federal University of Ceará, Fortaleza, Ceará 60455-900, Brazil

2017; Zhang et al. 2019). Spatiotemporal analysis of precipitation is key to water resources risk assessment. As precipitation is characterized by volatility, variability, and geographical differentiation, its analysis can be challenging. Also, data availability might be an issue in some regions (Eris et al. 2020). Therefore, the topic of spatiotemporal variation of precipitation has received increased attention, particularly in arid and semi-arid regions. This type of analysis has been performed considering different spatial scales such as a country or a group of countries (Qin et al. 2018), a state or province (Meshram et al. 2017; Tongal and Sivakumar 2019; Jhong et al. 2019; Yang et al. 2019a; Villalta et al. 2020), a region (Cunha et al. 2018; Fu et al. 2021), or a river basin (Zhou et al. 2013; Li et al. 2016; Liu et al. 2016; Ahmad et al. 2018; Yang et al. 2019b).

The study of complexity in precipitation is the basis for regional risk assessment and water resources management. Several literature methods measure the variability of a time series, including variance, regression analysis, nonparametric tests, diversity indices, and information-theory-based measures (Zhang et al. 2019). However, regression methods, for example, only measure the regularity of precipitation and may not quantify the degree of this disorderly change. Thus, these methods cannot effectively characterize the inherent complex changes of precipitation.

The information-theory-based measure, entropy (Shannon 1948), has gained significant attention in water resources studies in recent years (Zhang et al. 2019). A change in entropy values is related to the information transmitted or gained, allowing inferences about a variable. Thus, the entropy-based approach is likely to characterize the variability and uncertainty inherent in water resource dynamics. The disorderly changes in precipitation can impact regional flooding and droughts, water resources, and socioeconomic activities. Studies regarding precipitation variation become critical in semi-arid regions because of different types of water demands during distinct months and seasons. Furthermore, investigating the seasonal distribution of precipitation is particularly important for the rational allocation of water resources.

Approaches based on entropy theory generally employ spatiotemporal concepts to measure information, disorder, or uncertainty without strict assumptions about statistical properties or probability distributions of the data, thus being applied to any data and any system (Su and You 2014; Tongal and Sivakumar 2019). In the hydrology context, entropy-based methods have been used in assessing the variability of rainfall (Mishra et al. 2009; Zhang et al. 2016; Guo et al. 2017), streamflow and runoff (Maurer et al. 2004; Roushangar and Alizadeh 2018), rainfall network design (Su and You 2014), regionalization and clustering of catchments (Agarwal et al. 2016; Tongal and Sivakumar 2019), and water resources availability (Da Silva et al. 2016). Most of these methods have used non-normalized indices to estimate rainfall variability. Hence, the outcomes cannot be used for comparison at different timescales and different data lengths.

The purpose of this study is to assess the underlying spatiotemporal disorder or variability by using standard variability indices (SVI). The indices assess changes in rainfall uncertainties and complexities at different timescales. Generally, studies in the region are more focused on assessing trends in single or multiple climate variables through different timescales (Santos et al. 2009; Costa and Silva, 2017; Ferreira et al. 2018), and less attention has been given to evaluating the complexity characteristics of the climate system. Due to the climate system's nonlinear and nonstationary behavior, an exploration of its inherent complexity has theoretical and practical relevance for revealing the uncertainty and variability of the system. Also, variability information has the potential to be used in developing strategic adaptation and mitigation measures aimed at improving the resilience of water systems. The analyses were applied to the State of Ceará, located in NEB. Ceará was chosen because of its history of severe and sometimes multi-annual droughts. These multi-annual events impose challenges and weaknesses in the water resource system and reveal the importance of studies on the uncertainties in hydrological variables to improve the planning of water resources.

The specific objectives of the present study are: (1) to assess the spatiotemporal rainfall variability at different timescales (e.g., daily, monthly, and annual), (2) to investigate the intra-annual and the decadal distribution of rainfall variability and compare the different periods, (3) to investigate the relation of variability between rainfall and streamflow, and (4) to explore the trends and significance of intra-annual variability. Shannon's entropy (Shannon 1948) was applied to analyze the variability patterns of rainfall. Then, the entropy is standardized using Guntu et al. (2020) methodology. Long-term trends were assessed at daily, monthly, and seasonal scales using the Mann–Kendall test and the Sen's slope estimation method (Kendall 1948; Mann 1945; Sen 1968). The kriging method was employed to spatially delineate the variability of entropy (Krige 1966). This application will be useful to improve the understanding of rainfall characteristics and formulate interferences on climate variability in a semi-arid region.

2 Study area and hydrological data

The State of Ceará is located in the semi-arid region of NEB. The Brazilian semi-arid region is the world's most densely populated dryland region. The economy is mainly

based on agricultural production, which is intrinsically dependent on the region's rainfall. Several large-scale mechanisms influence NEB precipitation. Global and regional climate change scenarios indicate that the region will be affected by rainfall deficit and increased aridity in the next century (Marengo et al. 2017).

The rainfall regime in Ceará State is characterized by high spatiotemporal variability, with over 60% of the total rainfall (about 650 mm per year on average) occurring from February to May (Alves et al. 2009). The rainfall pattern is directly linked to the Intertropical Convergence Zone (ITCZ) movement, which reaches its Southernmost position during March and April. Also, rainfall patterns are modulated by the natural fluctuations of the sea surface temperature (SST). Climate indices such as the El Niño Southern Oscillation (ENSO) phenomenon, the Pacific Decadal Oscillation (PDO), and the Atlantic Multidecadal Oscillation (AMO) have been reported to directly impact the NEB rainfall regime (Andreoli and Kayano 2005; Garreaud et al. 2009; Kayano et al. 2020).

The analysis of the spatiotemporal variability of the rainfall regime considered data from the Brazilian National Water Agency (ANA). Time series are comprised of daily data from January 1962 to December 2006. This study considered 31 meteorological stations around the State of Ceará, illustrated in Fig. 1. The basic statistical properties about the annual total precipitation amount and monthly total precipitation amount for the stations are listed in Table 1. To present the distribution characteristics of the rainfall data at an annual scale, violin plots were plotted. There is also information about the median, the quartiles (25 and 75%), and outliers (see Fig. 2). These representations allow us to distinguish the internal variability that rainfall presents in each of the stations. The stations located in the Northern region of the State had the greatest variability. The most extreme case was reached by Station 4 with a range between 465 and 2311 mm, followed by Stations 9 and 16. Stations located more to the Central and Northeastern portion of the State shown a violin plot that is thick at its centre because of its small range of values. Further, most of the density plots showed a unimodal shape, however, Station 24 presented a bimodal shape. Streamflow data from 1963 to 2006 was also acquired from ANA to calculate the relation of rainfall and streamflow variability. In order to investigate the connection between intra-annual variability and large-scale indices, the Oceanic Niño Index (ONI) was used. The ONI is applied by US National Oceanic and Atmospheric Administration (NOAA) to monitor the ENSO phenomenon. The index consists of a 3-month running mean of the average sea surface temperatures in the east-central tropical Pacific between 120°-170°W, which is the Niño 3.4 region. The ONI data was acquired from the database through the climate prediction center website (https:// https://www.cpc.ncep.noaa.gov/products/precip/CWlink/MJO/enso. shtml, data retrieved in June of 2021).

3 Methods

In this study, the concept of entropy and SVI, as discussed by Guntu et al. (2020), are applied to analyze the spatiotemporal variability/uncertainty of rainfall time series in multiple timescales (e.g., monthly, seasonal and annual). Three entropy-based measures (marginal entropy (ME), apportionment entropy (AE), and intensity entropy (IE)) are employed in the analysis. Further, the variability of rainfall is also compared within different decades. The

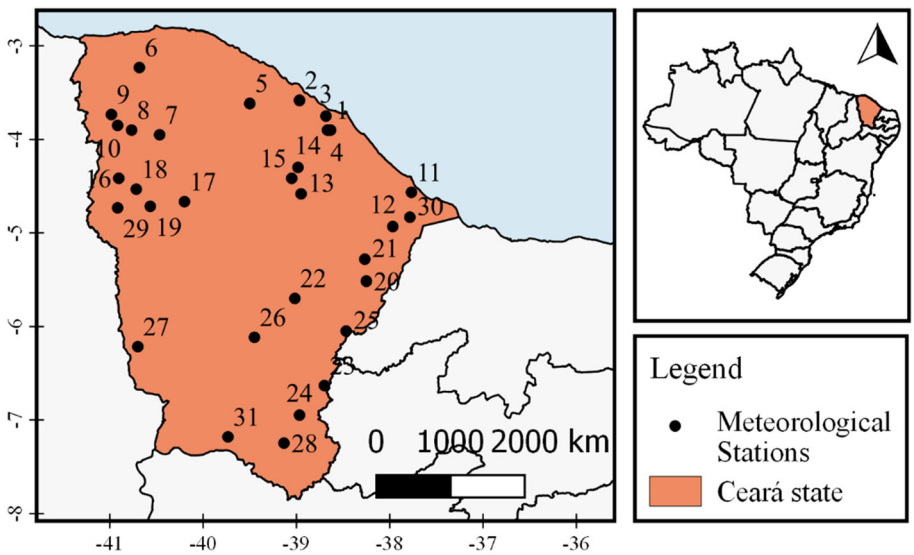

Fig. 1 Location of the meteorological stations analyzed in this study

Table 1 Statistical properties of annual/monthly precipitation time series (1962–2006) of the 31 analyzed stations

Station Number	Station ID	Min	Max	Mean	Standard Deviation
1	338,005	595.6/0	2778.5/582.6	1329.9 / 110.82	515.73/131.46
2	338,008	434.1/0	2200.3/635.9	1075.89 / 89.66	421.67/118.43
3	338,009	675.5/0	2418.6/842.6	1334.17 / 111.18	465.19/138.46
4	338,016	465.2/0	2311.7/523.7	1252.4/ 104.37	434.74/121.94
5	339,034	419/0	2061.8/637.9	1177.06 / 98.09	395.73/125.85
6	340,008	399.8/0	2186.7/642.5	1105.53 / 92.13	407.56/128.44
7	340,014	260/0	1723/619	942.75 / 78.56	349.05/113.66
8	340,023	476.6/0	2120.8/642	1038.28 / 86.52	375.19/114.91
9	340,030	469.5/0	2409.3/753.4	1257.18 / 104.76	418.27/132.14
10	340,031	664.7/0	2864.5/724.8	1516.85/ 126.4	513.42/153.09
11	437,000	220/0	2654.1/650.5	983.26 / 81.94	501.8/118.96
12	437,010	173.4/0	1929.1/502.4	769.85 / 64.15	311.9/91.64
13	438,032	284.2/0	1573/391	786.17/ 65.51	278.97/85.05
14	439,008	479.1/0	2149.9/457.2	1191.1/ 99.26	399.21/105.78
15	439,018	416.3/0	3238.2/788.3	1456.66 / 121.39	647.5/139.65
16	440,005	154/0	1116.8/492.1	575.1 / 47.92	228.64/72.78
17	440,009	27.1/0	1987.7/639.7	710.68 / 59.22	327.38/95.36
18	440,014	280.5/0	2004.2/568.6	967.15 / 80.6	381.55/113.66
19	440,017	351/0	1703.4/550	868.26 / 72.36	339.54/107.34
20	538,003	116.7/0	1823.9/490.8	772.66 / 64.39	289.75/91.19
21	538,010	268/0	1852.5/567.8	777.97 / 64.83	321.03/89.01
22	539,023	237.2/0	1375.8/461.6	783.86 / 65.32	247.16/85.55
23	638,008	390.8/0	1702.6/474.9	794.04 / 66.17	240.07/86.66
24	638,010	517.8/0	1951/653	926.33 / 77.19	283.84/103.85
25	638,011	294.6/0	2065.7/537.5	1016.64 / 84.72	359.87/108.88
26	639,021	366/0	1713/517	798.02 / 66.5	251.56/87.55
27	640,015	266/0	2237.1/950.1	697.94 / 58.16	333.61/92.25
28	739,007	594/0	1885.6/550	1006.15 / 83.85	267.79/107.87
29	440,018	144/0	1262.8/469.8	650.49 / 54.21	276.97/79.59
30	437,006	118/0	1887.7/629.2	824.78 / 68.73	416.58/108.4
31	739,005	304.4/0	1612.1/589.1	920.56 / 76.71	278.81/100.32

Mann–Kendall and Sen's slope tests are applied to assess significant trends in the SVI. The rainfall and streamflow variability for a station is also calculated and compared in different timescales. In addition, maps are constructed with the kriging method to delineate the SVI's spatial patterns. The methods are summarized in Fig. 3, and a brief description of these methods is presented in the following sections.

3.1 Shannon entropy

Entropy is a measure of dispersion, uncertainty, disorder, and diversification (Mishra et al., 2009). Shannon's entropy (1948) in a discrete form can be expressed as:

$$H(X) = -\sum_{k=1}^{K} \mathrm{p}(\mathrm{x}_k)\log(\mathrm{p}(\mathrm{x}_k)) \quad (1)$$

Where $H(X)$ is a measure of the information associated with the underlying process, k denotes a discrete interval, and $\mathrm{p}(\mathrm{x}_k)$ is the probability density function of the variable x. The unit of H can be bits when the log function is taken to be $\log_2$, and can also be expressed in 'nats' in which the log function is taken as ln. The $\log_2$ function was used for the entropy measures computations in this study.

If all states are equiprobable or there is more evenness in the probabilities of random values, then H reaches its maximum value and it expresses the uncertainty about the system's state. However, if H equals to zero, then the probability of a certain state is 1, and complete information about a random variable is available. Thus, the entropy value can vary from zero to $\log_2 K$, where zero represents maximum certainty and $\log_2 K$ maximum uncertainty. With entropy reaching its maximum value, there is no indication

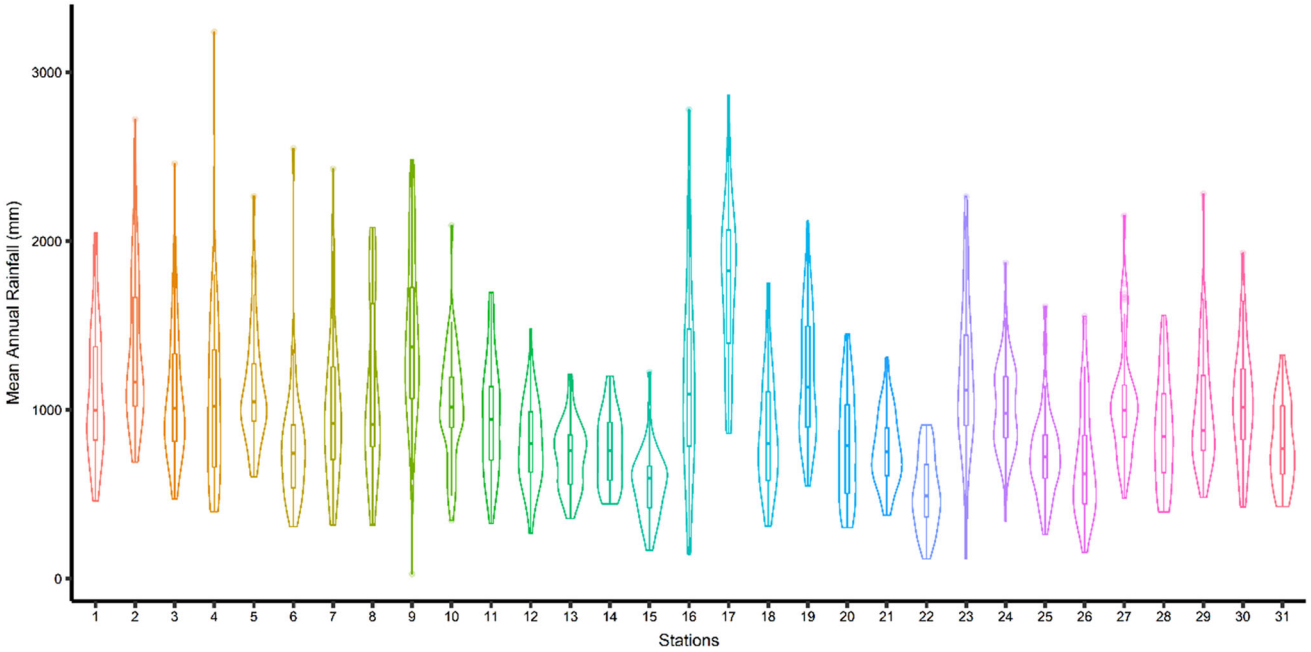

Fig. 2 Violin plots comparing the median, the spread, and the probability density function of rainfall data from the 31 analyzed stations. The median is shown by the horizontal line on the boxplot inside the violin plot and the maximum and minimum values are represented by points in the top and bottom of the plots, respectively

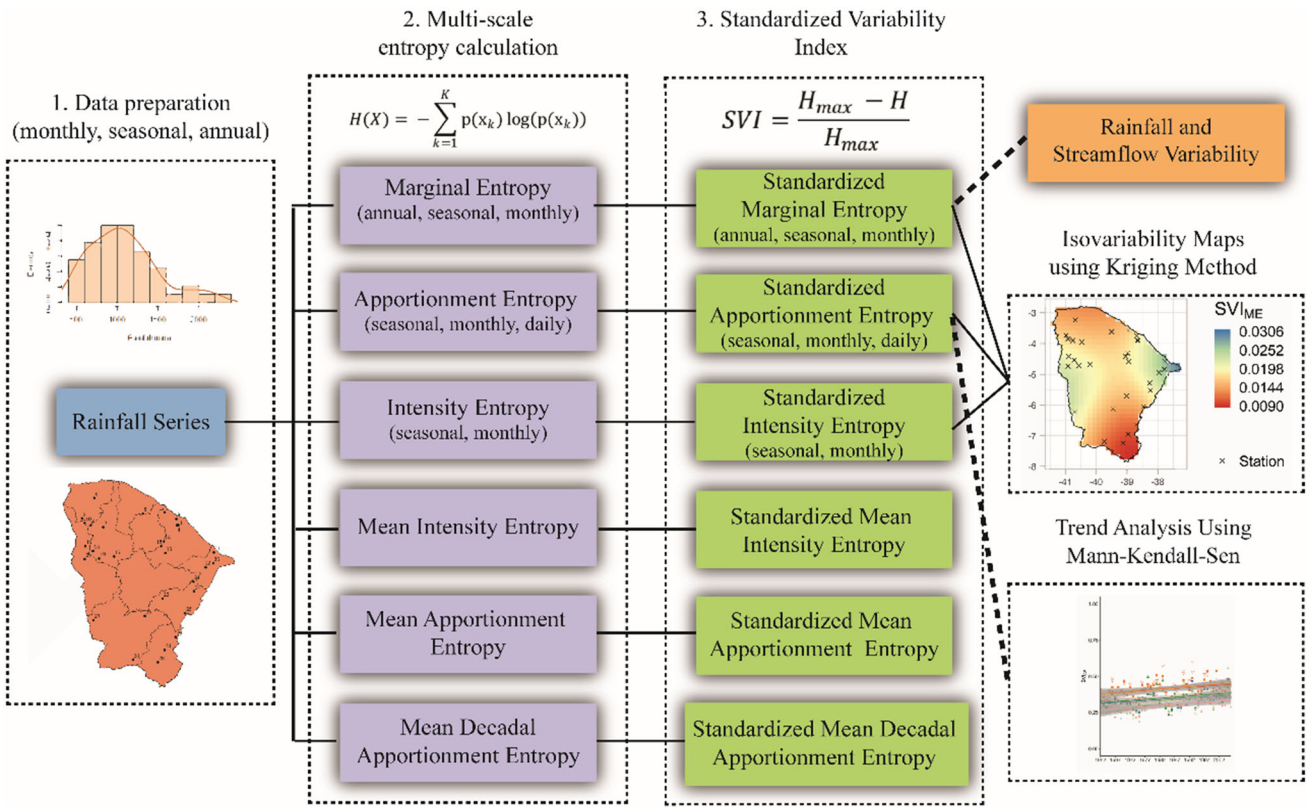

Fig. 3 The overall process of the spatiotemporal characterization of the Ceará State using entropy theory

to assume that one state is more probable than another state (Da Silva et al. 2016).

3.2 Standardized variability index (SVI)

The SVI proposed by Guntu et al. (2020) measures the variability of an individual series regarding the maximum possible variability. SVI can be defined as:

$$SVI = \frac{H_{max} - H}{H_{max}} \tag{2}$$

Where H_{max} is the maximum possible entropy and H is the entropy obtained for a given time series. H_{max} is equal to $\log_2 K$, and it depends on the length of the time series and the timescale. SVI can range from zero to one, where zero represents no variability and one represents high variability, i.e., maximum certainty to maximum uncertainty. Consequently, SVI can be used to compare the rainfall variability at distinct locations and different timescales on a fixed scale (Guntu et al. 2020).

3.3 Marginal entropy (ME)

ME is a measure of uncertainty or ignorance about the system's state. This index can be defined as the average information content of a random process (Da Silva et al. 2016; Cheng et al. 2017). For example, when the ME is calculated considering the historical monthly time series of a station, it results in the randomness associated with the entire length of the time series. ME can be used for annual, monthly, seasonal, and rainy days to assess the randomness in the time series (Mishra et al. 2009). ME is applied to the rainfall data from the analyzed stations at three different timescales, i.e., annual, seasonal, and monthly.

3.4 Apportionment entropy (AE)

The AE, as defined by Maruyama et al. (2005), measures the temporal variability of rainfall amount in terms of daily/monthly/seasonal timescales within a given year. The AE is estimated for each year at all meteorological stations according to:

$$AE = -\sum_{k=1}^{K} \left(\frac{r_k}{R}\right) \log_2 \left(\frac{r_k}{R}\right) \tag{3}$$

where R is the total amount of rainfall for a given year, r_k is the rainfall amount during the considered timescale for the corresponding year, and K is the number of class intervals.

For example, at the monthly timescale, AE becomes maximum ($H = \log_2 12$) when the annual precipitation amount is equally likely apportioned to each of the 12 months, having a probability of 1/12. The minimum value occurs when the apportionment is made to only one out of the 12 months, having a probability of 1. Thus, AE takes on a value within a finite range of 0 and $\log_2 12$ at a monthly timescale.

3.5 Intensity entropy (IE)

IE measures the rainy days' variability of a month or a season within a year to the total number of rainy days in that year. The IE is estimated for each year at all meteorological stations using:

$$IE = -\sum_{k=1}^{K} \left(\frac{m_k}{M}\right) \log_2 \left(\frac{m_k}{M}\right) \tag{4}$$

where m_k is the number of rainy days within a month or a season, M is the total number of rainy days in that year, and K is the number of class intervals. For instance, $K = 12$ for monthly timescale. In this study, IE is used to measure the intra-annual variability in terms of intra-annual rainy day's distribution.

3.6 Trend Analysis using Mann–Kendall and Sen's slope methods

The Mann–Kendall (Kendall 1948; Mann 1945) is a non-parametric test widely used in environmental and hydrological time series. In this study, the test is applied to detect trends in the SVI calculated from precipitation data. The null hypothesis employed in the test assumes that the data came from a population with independent and identically distributed realizations. The test's null hypothesis was accepted if the p-value was less than the significance level of 0.05, detecting either increasing or decreasing monotonic trends. Sen's slope estimator was used to quantify the magnitude of the trend according to Sen's method (Sen 1968).

4 Kriging method

Spatial interpolation techniques have been applied to assess the magnitude and variability of parameters. The geostatistical (or stochastic) methods, such as ordinary kriging, provide prediction surfaces with error estimates of measured data based on their statistical properties (Eldrandaly and Abu-Zaid 2011). The kriging method uses a semivariogram and a covariance function to predict unmeasured locations by creating continuous surfaces.

In the kriging procedure, the empirical semi-variogram is calculated by computing locations within a distance interval for pairs of observations. The empirical semivariogram indicates how the dissimilarity between points

evolves with distance. In order to obtain spatial predictions, a continuous function or curve should be fitted to the empirical semi-variogram. The theoretical semi-variogram model provides the information regarding the spatial variability that is required for the kriging method. Several theoretical semi-variogram functions are available, such as spherical, circular, exponential, and Gaussian models. Spatial inference of a quantity at an unobserved location is calculated from a linear combination of the observed values and weights. The weights are generated from the variogram model fit that represents the spatial correlation structure of data to ensure that the estimator is unbiased with minimum variance.

In this study, different theoretical semi-variograms, mentioned above, are examined. The model that has the smallest residual sum of squares errors with the empirical semi-variogram is selected. Then, cross-validation tests for the kriging predictions of all entropy measures are performed to give a more accurate estimate of the model's prediction performance. A sample of the entropy measure is removed individually and estimated from the remaining measures. The mean standard error (MSE) and mean square standard error (MSSE) are used to evaluate the model prediction performance. The calculated values of MSE and MSSE for the annual SVI_{ME} and mean annual rainfall are close to zero and one (see Appendix 1), with values within the accepted tolerance error of $\pm 3(2/n)0.5$, as Liang et al. (2019) recommended.

5 Results and discussion

5.1 Variability of annual, seasonal, and monthly rainfall

In this study, ME, AE, and IE are expressed in SVI terms and are denoted as SVI_{ME}, SVI_{AE}, and SVI_{IE}, respectively. In order to investigate the variability of annual, seasonal, and monthly rainfall time series, the ME and SVI_{ME} are calculated based on the amount of rainfall for each considered station. Figure 4 shows the computed SVI_{ME} for annual, seasonal (rainy and dry), and monthly rainfall time series over different meteorological stations. When comparing seasonal results, the SVI_{ME} from the dry season (July to December) had the highest value, which indicates a greater variability associated with the analyzed stations in that season. The SVI_{ME} for Station 16 showed higher mean values in the annual, rainy season, and monthly analysis, followed by Station 17. Both stations are located in the State's Western region.

Figure 5a shows the spatial distribution of the mean SVI_{ME} for annual rainfall time series (1962–2006) over the different stations. The SVI_{ME} represents the variability obtained from the maximum possible variability associated with each station. Overall, the SVI_{ME} at the annual timescale showed lower values in the Southern and Northern regions, while the Eastern region presented higher values of variability. In comparison, the mean annual rainfall (Fig. 5b) followed a smooth contour with a decreasing pattern from North to South. Meteorological stations with high variability are observed in the low rainfall regions and vice-versa. Results show that the nature of mean annual rainfall can vary from the SVI_{ME} associated with it on a spatial scale. In general, meteorological stations in the Eastern region had the highest variability, which coincides with low rainfall. Although stations with low variability are identified in the Southeastern region and on the Northwest Coast, only the Northwestern area coincided with high rainfall.

5.1.1 .

Similarly, SVI_{ME} is also spatially distributed for rainfall at the seasonal (rainy and dry) and monthly timescales. Figure 6 presents the spatial distribution of SVI_{ME} at a seasonal scale, and Fig. 7 shows the spatial distribution at a monthly timescale. The cross-validation tests for the monthly kriging approach for June, July, and October produced MSE values close to zero, however, the MSSE was outside the range of the tolerance error (see Appendix 1). Table 2 presents the statistical properties of SVI_{ME} for seasonal and monthly time series. In the rainy season (from January to June), the State had lower variability than the dry season (from July to December). This result is also observed in Fig. 3, and that behavior is related to the regular rainfall at this season, which is influenced by the position of the ITCZ (Kayano and Andreoli 2006). In addition, the rainy season variability map resembles the mean annual rainfall map (Fig. 5b), which shows the influence of rainfall concentrated only in this part of the year. However, in the dry season, the State receives unseasonal rain with no uniform pattern causing high variability in its spatial extent. Thus, the dry season contributes most to the annual relative variability. Noteworthy, even though most of the annual rainfall comes from the rainy season, the annual rainfall variability is contributed mainly by the dry season. Similar conclusions were drawn by Guntu et al. (2020) and Da Silva et al. (2016).

When individual months are compared, the month(s) responsible for the seasonal variability can be assessed, and consequently, the intra-variability of months within a season. The results showed that high SVI_{ME} values could be observed in August throughout November. Thus, variability is higher in the individual months than in the season. According to Mishra et al. (2009), intra-annual variability will be more substantial at a smaller timescale

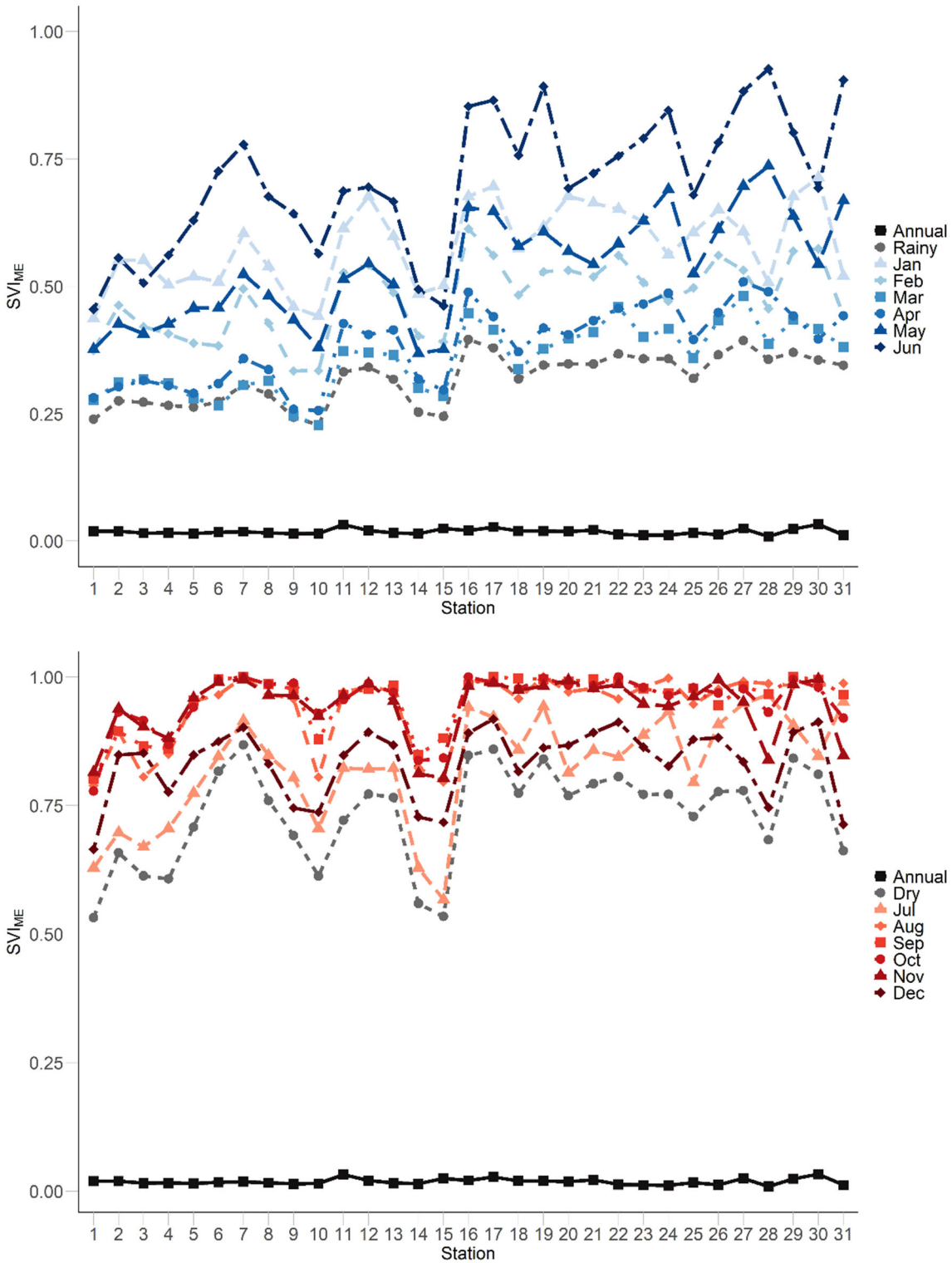

Fig. 4 Mean SVI_{ME} for annual, seasonal, and monthly rainfall time series of the analyzed stations

and becomes smaller at a larger timescale, as observed in our results. From the stations' analysis at a monthly timescale, Stations 16 (Western region) showed greater variability values from January to June. Station 17 presented the highest values from July to December. Station 1 (Northern region) showed the lowest values for January and June, and also for July and December.

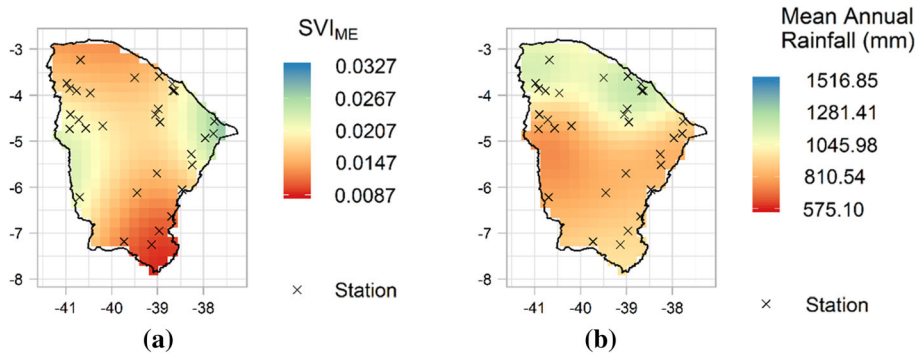

Fig. 5 Spatial distribution of **a** mean annual SVI_{ME}, and **b** mean annual rainfall over the period 1962–2006

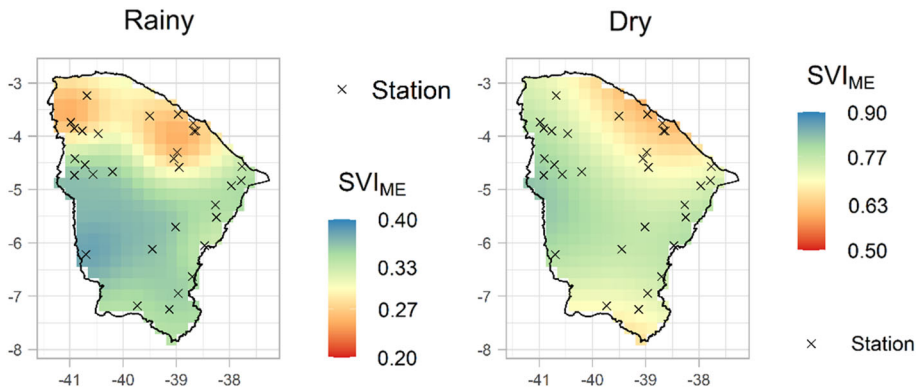

Fig. 6 Spatial distribution of rainfall seasonal variability over the period 1962–2006 based on SVI_{ME}

Figure 7 shows that the Southern region and the Central portion of the State presented higher values of SVI_{ME} during July throughout December, which corresponds to the considered dry season in this study. The State's Central region is strongly influenced by semi-arid climate conditions, with low rainfall during a short period of the year and prolonged dry seasons. On the other hand, February, March, April, and May showed relatively low values of the SVI_{ME}, suggesting lower uncertainty associated with the State's rainfall season. In December, there was a decrease in the SVI_{ME} in the far South of the State related to the higher altitude of Chapada do Araripe, which conditions greater humidity and causes orographic rainfall. Furthermore, this pattern was captured in the State's Southern region on an annual timescale for SVI_{ME}. The Southern region presented an opposite behavior to the rest of the state (low rainfall was related to the high variability and vice versa). In this region, there are orographic rainfalls associated with the region's topography, and the low variability captured the presence of that rainfall. However, compared to the rainfall intervals of the State's Northern region, the Southern region presented average to low precipitation. Thus, due to intra-annual variability, the annual scale did not represent the variability of rainfall that the State has so well.

5.2 Variability of rainfall apportionment and intensity

After examining the variability of rainfall amount for annual, seasonal, and monthly time series, it is necessary to investigate the variability of rainfall distribution within a year regarding the amount and the number of rainy days. The AE and the SVI_{AE} are calculated at daily, monthly, and seasonal timescales. Additionally, the IE and the SVI_{IE} are calculated at monthly and seasonal timescales for every rainfall station covering the entire length of the time series data (1962–2006).

Figure 8 shows that the mean SVI_{AE} for the studied period at the daily timescale presented a lower variability in the Northwestern and North Coast regions. This result indicates the concentration of rainfall throughout the year, which is generally the situation in the coastal region of the State. The mean daily SVI_{AE} for the other parts of the State presented a homogenous pattern characterized by rainfall concentration during only a few days of the year. At the monthly scale, locations with low variability extended to the Southern and Central regions, indicating that rainfall in a major part of the State is scarce for most months. At the seasonal scale, the state showed high variability in the range of 0.4–0.8, with a mean value of 0.63 (see Fig. 8 and Table 3). This result indicates that the rainfall variability pattern becomes more prominent when the timescale

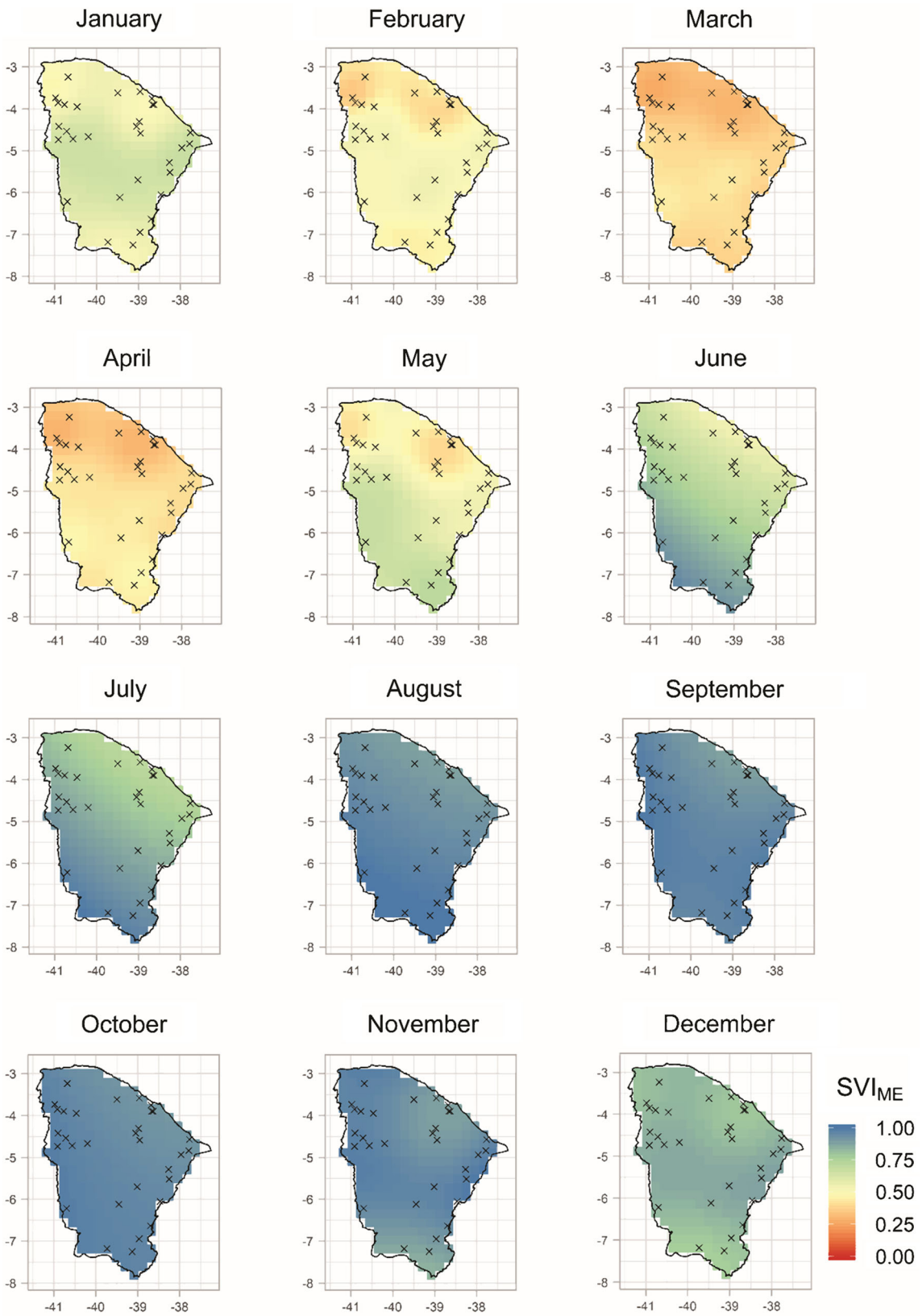

Fig. 7 Spatial distribution of rainfall variability for monthly timescale over the period 1962–2006 based on SVI_{ME}

Table 2 Statistical properties of SVI_{ME} for seasonal and monthly time series

	Min	Max	Mean	Std. dev	Range	
Month	January	0.139	1.000	0.581	0.196	0.860
	February	0.113	1.000	0.476	0.180	0.886
	March	0.091	1.000	0.357	0.132	0.908
	April	0.095	1.000	0.385	0.160	0.904
	May	0.117	1.000	0.535	0.218	0.883
	June	0.161	1.000	0.707	0.238	0.838
	July	0.183	1.000	0.825	0.205	0.817
	August	0.388	1.000	0.942	0.124	0.612
	September	0.030	1.000	0.955	0.112	0.699
	October	0.347	1.000	0.953	0.113	0.653
	November	0.339	1.000	0.942	0.126	0.661
	December	0.174	1.000	0.833	0.188	0.826
Season	Rainy	0.140	1.000	0.581	0.196	0.860
	Dry	0.113	1.000	0.476	0.181	0.887

changes from finer to coarser. Similar results were found in Guntu et al. 2020. In addition, for the SVI_{AE} at the daily and monthly scales, the mean value is found to increase from the West and East to the Central portion of the State. However, the opposite occurred in the seasonal timescale. This pattern can be attributed to the significant uneven rainfall distribution in the Central portion of the State over the year, thus leading to remarkably high values of intra-annual variability.

When looking at the variability over the years (Fig. 9a), the first eight years presented values below the long-term average. From 1975, there was a cyclical variation of two to four years. In order to assess the relation between rainfall variability patterns and SST oscillation, the mean annual ONI, applied by NOAA to monitor the ENSO events was plotted against the SVI values. If the ONI is

Table 3 Statistical properties of Standardized Variability Index based on Apportionment Entropy of rainfall distribution

	Min	Max	Mean	Std. dev	Range
Daily	0.185	0.864	0.380	0.075	0.679
Monthly	0.096	1.000	0.311	0.091	0.904
Season	0.040	1.000	0.627	0.230	0.960

greater than + 0.5 °C, (lower than − 0.5 °C) an event is classified as El Niño (La Niña). Results showed that some years with higher SVI_{AE} were also years with El Niño's presence (e.g., 1963, 1965, 1982, 1987, 1991, 1992, 1997, 2002). This result corroborates the influence that this anomaly has over the studied region. During the El Niño years, the precipitation is scarce, thus resulting in higher variability. The same occurs for years that presented La Nina events (e.g., 1973–1975, 1985, 1988–1989, and 1999–2000.

The number of rainy days at different timescales plays a significant role in water resource planning. Hence, the IE and the SVI_{IE} are calculated. The spatial distribution of the mean $SVI_{IE,}$ at the monthly scale, showed that low variability is concentrated throughout the State (Fig. 10). At the seasonal scale, high variability regions are located in the Northwestern region. The SVI_{IE} pattern presented similarities to the SVI_{AE} at both timescales analyzed.

The variability in terms of SVI_{IE} indicates that the rainy days are concentrated only within a certain period of the year for high variability. In contrast, low variability means that the rainy days are distributed or scattered across the year (Guntu et al. 2020). Further, in the monthly timescale, the rainfall is distributed across the year. However, on a seasonal scale, rainfall is concentrated only within a specified period. Thus, the mean values of SVI_{IE} indicated that the variability is higher at the seasonal timescale

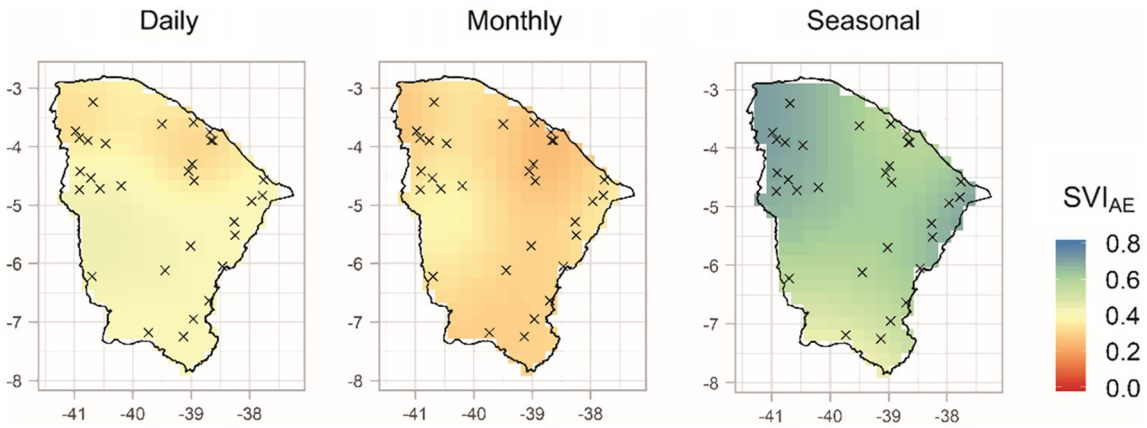

Fig. 8 Spatial distribution of rainfall variability at different timescales based on SVI_{AE}

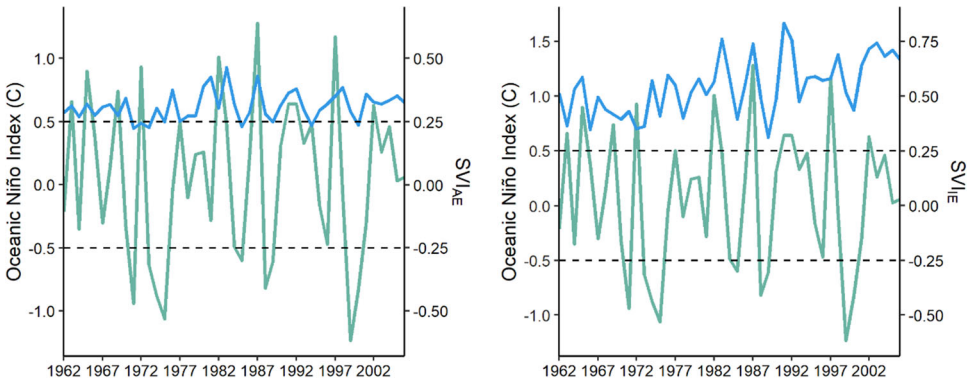

Fig. 9 Mean **a** SVI_{AE} (blue line), and **b** SVI_{IE} (blue line) of rainfall time series of all stations for the period of 1962–2006 and ONI (green line) with the dashed lines indicating the limit to consider El Niño (+ 0.5 °C) or La Niña (−0.5 °C) conditions

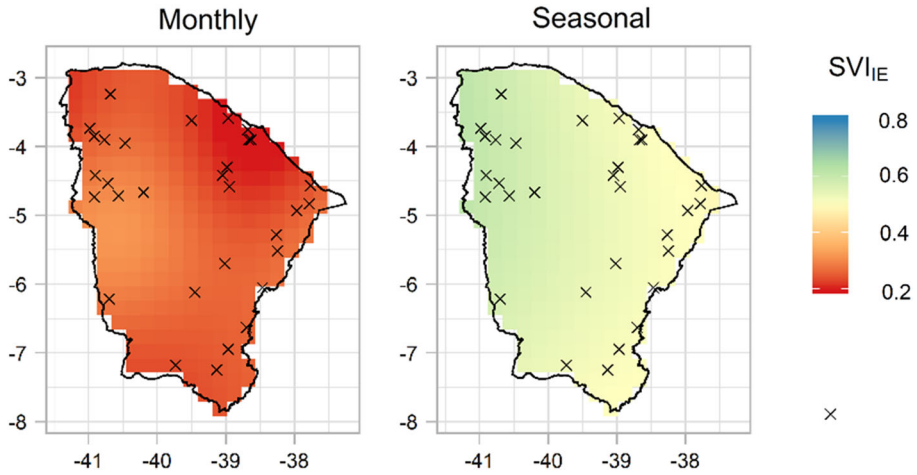

Fig. 10 – Spatial distribution of rainfall variability at different timescales based on SVIIE

compared to the monthly timescale (see Table 4). When analyzing the SVI_{IE} throughout the years (Fig. 9b), a relatively lower SVI_{IE} is observed in the first two decades, similarly to the $SVI_{AE.}$ According to Cheng et al. (2017), one explanation for this is that there are more zero values in rainfall records. When analyzing the SVI_{IE} and the ONI, the same relation is also observed between intense El Niño events (+ 1.0 °C) and higher values of SVI_{IE} (e.g., 1982, 1987, and 1997). Depending on the intensity of the El Niño event, there may be inhibition in the formation and descent of the ITCZ and, consequently, there may be a deficiency of rainfall in the NEB region. Thus, the rainy days are more concentrated in a part of the year. Overall, based on SVI_{AE} and SVI_{IE} values, the State's Coastal North area presented low variability at the monthly and seasonal timescales, which is consistent since that area receives a reasonable amount of rainfall throughout the year. The variability patterns were different at all timescales analyzed (daily, monthly, and seasonal), highlighting the multiscale variability of the rainfall pattern. Thus, the intra-annual variability varies from scale to scale.

Table 4 Statistical properties of Standardized Variability Index based on Intensity Entropy of rainfall distribution

	Min	Max	Mean	Std. dev	Range
Monthly	0.020	1.000	0.254	0.095	0.980
Season	0.017	1.000	0.552	0.243	0.983

5.3 Decadal Variability of Rainfall

In order to verify the variability over more extended periods, the decadal SVI_{AE} and the decadal SVI_{IE} were calculated. Figure 11 shows the mean decadal entropy values for the different timescales (e.g., daily, monthly, and seasonal), as for the individual months. For the rainfall amount, the first decade (1967–1976) had a lower variability at the daily, monthly, and seasonal timescales than the other decades. In contrast, the last decade presented the lowest variability in January. From June to December, the variability became almost the same. Thus, it is possible to say that the temporal variability of rainfall amount varies with the timescale and with the decades. The influence of the changes in rainfall variability might also be linked to climate indices with decadal variability. For instance, the PDO is in its cold phase from 1967–1976, and there is a

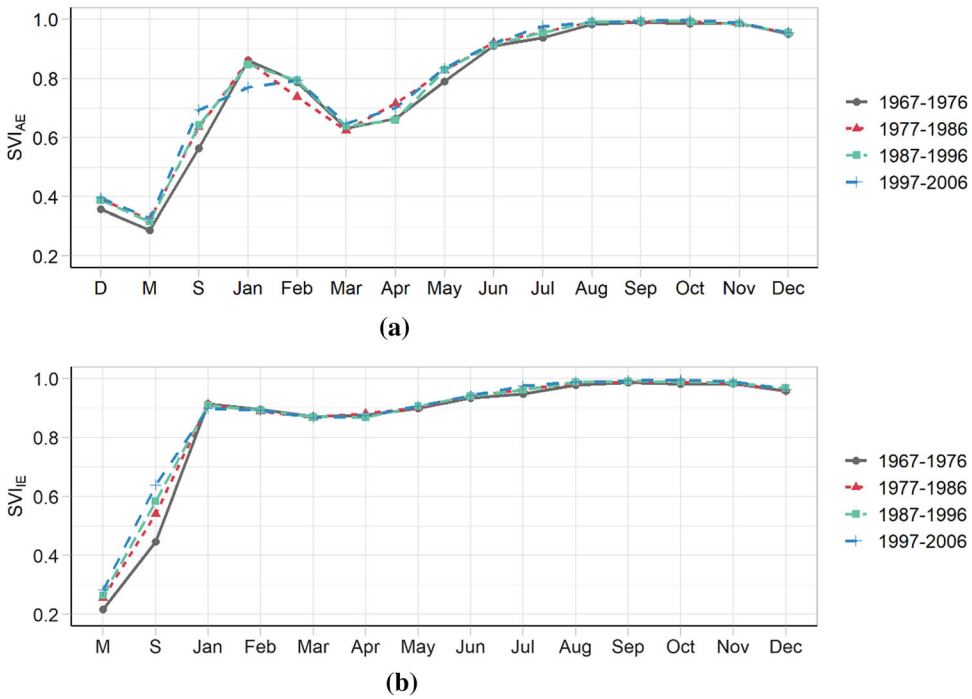

Fig. 11 – Mean decadal **a** SVIAE and **b** SVIIE of rainfall time series at different timescales. D, M and S refer to daily, monthly, and seasonal timescale, respectively

shift to its warm phase (1977–1996). Many studies have linked climate indices with decadal variability to the rainfall patterns in NEB (Andreoli and Kayano 2005; Kayano and Andreoli 2006; Garreaud et al. 2009; Kayano et al. 2020). The variability of rainfall rainy days showed similarities in the first decade at the monthly timescale. At the seasonal analysis, there was a slight reduction in rainfall over the decades. However, for the individual months' analysis, this reduction seemed to occur homogeneously throughout the months.

5.4 Trend analysis of apportionment entropy

The Mann–Kendall trend test is applied to evaluate the trends of SVI_{AE} from the 31 stations. The results showed that 26% of the stations presented a significant upward trend in the daily timescale. Figure 12 illustrates the upward trend at the analyzed locations, which indicates an increase in SVI_{AE} variability over the years. Thus, it is noted that rainfall gets more concentrated only during a certain period of the year. At the monthly timescale, 16% of the stations showed a significant upward trend. At the seasonal timescale, 32% of the stations presented a significant trend. According to Khan et al. (2016), as precipitation at a small timescale is more prominent, its trend characteristics may not be as significant as it is for longer timescales. Thus, the presence of significant trends at larger timescales indicates a significant increase in the variability in the area. There were no stations that presented a downward trend, which means no increase in the spread of rainfall within a year. At all timescales, the stations with positive trends were mostly concentrated in the Northern part of the State. This result can be attributed to the heterogeneity in rainfall over that State's area.

5.5 Relation of rainfall and streamflow variability

In order to evaluate the co-variability of different hydrological variables, the mean values of SVI_{ME} of rainfall and streamflow at a sample station (Station 16), located in the Western region of Ceará, were compared at annual and seasonal timescales (Table 5). Results showed that the SVI_{ME} values of rainfall and streamflow were lower during the rainy season, and the annual values were similar to the rainy season. The coefficient of variation (CV) was also calculated to verify the variability. The CV values were high for the streamflow time series, while the rainy season value was almost double the dry season. However, the maximum value was observed for the annual streamflow time series, reaching 336.1%. According to the CV results, the streamflow is more variable than the rainfall in the study area. Similar results were found by Da Silva et al. 2016, who studied the variability of rainfall using entropy in semi-arid areas of Brazil.

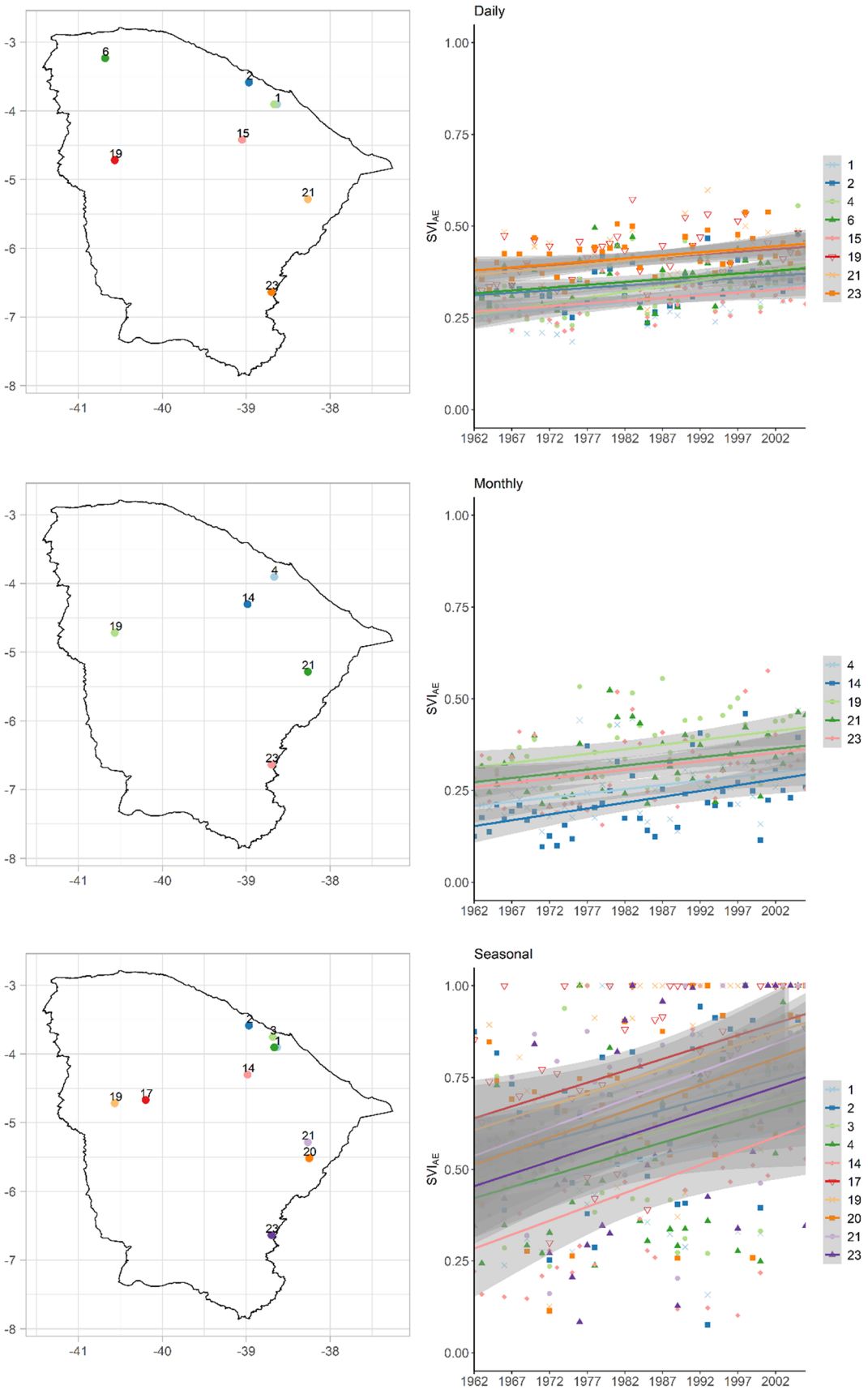
Daily
Monthly
Seasonal
SVI_AE
1.00
0.75
0.50
0.25
0.00
1962 1967 1972 1977 1982 1987 1992 1997 2002
-3
-4
-5
-6
-7
-8
-41 -40 -39 -38
1 2 4 6 15 19 21 23
4 14 19 21 23
1 2 3 4 14 17 19 20 21 23

◀**Fig. 12** Spatial pattern of meteorological stations that presented significant trends based on Mann Kendall test for SVIAE at daily, monthly, and seasonal timescales. The figures on the left show the location of the stations, and the figures on the right present the magnitude of the significant trend at the three timescales analyzed

Table 5 Mean values of standardized variability index for marginal entropy (SVI_{ME}) and the coefficient of variation (CV) for the annual and rainy and dry season rainfall and streamflow for station 16

	Rainfall			Streamflow		
	Annual	Rainy	Dry	Annual	Rainy	Dry
SVI_{ME}	0.363	0.20	0.80	0.328	0.41	0.52
CV (%)	39.9	94.1	279.23	336.1	218.8	132.22

6 Conclusions

This study aims to assess the underlying spatiotemporal variability in rainfall using SVI applied to a semi-arid region, which has been historically marked by severe and sometimes multi-annual droughts. The results showed lower variability in the State's North Coast region at all timescales and higher variability in the Eastern region for most of the analyses. Although high variability was found in areas with low rainfall amounts, this was not the case for the whole State. Spatial distributions of seasonal entropies revealed that the dry season contributes more to the annual variability. This fact can be attributed to the propagation of uncertainty due to the high spatiotemporal variability of the State's rainfall regime.

The rainfall variability pattern in the intra-annual analysis became more prominent as the timescales shifted. Furthermore, due to significant uneven rainfall, the intra-annual variability pattern can vary with timescales. Similarly, the relative intra-annual variability for rainy days showed that the rainfall was distributed across the year in the monthly timescale. While, at a seasonal scale, rainfall was concentrated only within a specified period. Thus, multi-scales analyses are necessary for comprehending the intra-annual variability of rainfall.

In the co-variability analysis, both rainfall and streamflow variability can be obtained to inferred regional uncertainty of hydrological events. When comparing two variability measures, the entropy-based method showed that these variables vary similarly, while CV implied that the streamflow varies much more at the annual timescale. Thus, proper application of variability indices is needed to draw more realistic assumptions regarding hydrological variables' variability. The trend test of SVI_{AE} showed stations with significant trends in the State's Northern region. Further, the State presented regions with an increase in the variability of rainfall. Also, there was an increase in variability amount and intensity throughout the decades at the monthly and seasonal timescales. The increase in variability over the State reveals the growth of uncertainty intrinsic to hydrological variables over different timescales. This information can be useful to improve the planning and managing of water resources in the region.

This study's outcomes offer further evidence as to the usefulness of the entropy-based methods for understanding the spatiotemporal variability of hydrological variables, such as rainfall, in the face of the occurrence of extreme events. Potential future directions would be to consider other entropy-based methods that incorporate rainfall and streamflow simultaneously, allowing to determine whether rainfall and streamflow carry the same information content at different timescales.

Appendix

A—Mean Standard Error (MSE) and Mean Square Standard Error (MSSE) of the Kriging prediction for the different timescales.

Timescale of the data	MSE	MSSE
Annual SVI_{ME}	0.020	0.975
Mean Annual Rainfall	0.023	0.914
SVI_{ME} for January	0.014	0.958
SVI_{ME} for February	−0.007	0.943
SVI_{ME} for March	0.005	1.076
SVI_{ME} for April	0.028	1.088
SVI_{ME} for May	−0.001	1.018
SVI_{ME} for June	0.007	1.499
SVI_{ME} for July	0.007	1.122
SVI_{ME} for August	0.022	0.964
SVI_{ME} for September	0.030	0.967
SVI_{ME} for October	−0.028	1.177
SVI_{ME} for November	−0.019	1.057
SVI_{ME} for December	0.047	0.953
SVI_{ME} for the rainy season	−0.017	0.990
SVI_{ME} for the dry season	0.015	1.009
Daily SVI_{AE}	0.025	0.954
Monthly SVI_{AE}	0.018	1.043
Seasonal SVI_{AE}	0.031	1.426
Monthly SVI_{IE}	0.067	1.098
Seasonal SVI_{IE}	−0.001	1.783

Acknowledgements This study was financed in part by the Conselho Nacional de Desenvolvimento Científico e Tecnológico—Brasil (CNPq), the Coordenação de Aperfeiçoamento de Pessoal de Nível Superior—Brasil (CAPES), and the Fundação Cearense de Apoio ao Desenvolvimento Científico e Tecnológico (FUNCAP).

Funding This study was financed in part by the Conselho Nacional de Desenvolvimento Científico e Tecnológico—Brasil (CNPq), the Coordenação de Aperfeiçoamento de Pessoal de Nível Superior—Brasil (CAPES), and the Fundação Cearense de Apoio ao Desenvolvimento Científico e Tecnológico (FUNCAP).

Data availability and material (data transparency) Data was retrieved from the Brazilian National Water Agency (ANA) at http://www.snirh.gov.br/hidroweb/.

Code availability (software application or custom code) The calculations and figures were made using the R software.

Declarations

Conflict of interest The authors declare that they have no conflict of interest.

References

Agarwal A, Maheswaran R, Sehgal V, Khosa R, Sivakumar B, Bernhofer C (2016) Hydrologic regionalization using wavelet-based multiscale entropy method. J Hydrol 538:22–32. https://doi.org/10.1016/j.jhydrol.2016.03.023

Ahmad I, Zhang F, Tayyab M, Anjum MN, Zaman M, Liu J, Farid HU, Saddique Q (2018) Spatiotemporal analysis of precipitation variability in annual, seasonal and extreme values over upper Indus River basin. Atmos Res 213:346–360. https://doi.org/10.1016/j.atmosres.2018.06.019

Alves JMB, Servain J, Campos JNB (2009) Relationship between ocean climatic variability and rain-fed agriculture in northeast Brazil. Clim Res 38(3):225–236. https://doi.org/10.3354/cr00786

Andreoli RV, Kayano MT (2005) ENSO-related rainfall anomalies in South America and associated circulation features during warm and cold Pacific decadal oscillation regimes. Int J Climatol 25(15):2017–2030. https://doi.org/10.1002/joc.1222

Cheng L, Niu J, Liao D (2017) Entropy-based investigation on the precipitation variability over the Hexi Corridor in China. Entropy 19(12):660. https://doi.org/10.3390/e19120660

Cirilo JA, Montenegro SMGL, Campos JNB (2017) The Issue of Water in the Brazilian Semi-Arid Region. In: Bicudo CEM, Tundisi JG, Scheuenstuhl MCB. (eds) Waters of Brazil. Springer, Cham, pp 59–71. https://doi.org/10.1007/978-3-319-41372-3_5

Costa JA, Silva DD (2017) Distribuição espaço-temporal do Índice de anomalia de chuva para o Estado do Ceará. R Bras Geogr 10(4):1002–1013. https://doi.org/10.26848/rbgf.v10.4.p1002-1013

Cunha APM, Tomasella J, Ribeiro-Neto GG, Brown M, Garcia SR, Brito SB, Carvalho MA (2018) Changes in the spatial–temporal patterns of droughts in the Brazilian Northeast. Atmos Sci Lett 19(10):e855. https://doi.org/10.1002/asl.855

Da Silva VDPR, Belo Filho AF, Almeida RSR, De Holanda RM, Campos JHBC (2016) Shannon information entropy for assessing space–time variability of rainfall and streamflow in semiarid region. Sci Total Environ 544:330–338. https://doi.org/10.1016/j.scitotenv.2015.11.082

De Jong P, Tanajura CAS, Sánchez AS, Dargaville R, Kiperstok A, Torres EA (2018) Hydroelectric production from Brazil's São Francisco River could cease due to climate change and inter-annual variability. Sci Total Environ 634:1540–1553. https://doi.org/10.1016/j.scitotenv.2018.03.256

Eldrandaly KA, Abu-Zaid MS (2011) Comparison of Six GIS-based spatial interpolation methods for estimating air temperature in Western Saudi Arabia. J Environ Infor 18:38–45. https://doi.org/10.3808/jei.201100197

Eris E, Cavus Y, Aksoy H, Burgan HI, Aksu H, Boyacioglu H (2020) Spatiotemporal analysis of meteorological drought over Kucuk Menderes River Basin in the Aegean Region of Turkey. Theor Appl Climatol 142:1515–1530. https://doi.org/10.1007/s00704-020-03384-0

Ferreira PS, Souza WMD, Silva JFD, Gomes VP (2018) Variabilidade Espaço-temporal das Tendências de Precipitação na Mesorregião Sul Cearense e sua Relação com as Anomalias de TSM. Rev Bras De Meteorol 33(1):141–152. https://doi.org/10.1590/0102-7786331006

Fu T, Gao H, Liang H, Liu J (2021) Spatio-temporal precipitation changes and their localized predictors in the Taihang Mountain region, North China. Stoch Environ Res Risk Assess 35:665–679. https://doi.org/10.1007/s00477-021-01970-w

Garreaud RD, Vuille M, Compagnucci R, Marengo J (2009) Present-day South American climate. Palaeogeogr Palaeoclimatol Palaeoecol 281(3–4):180–195. https://doi.org/10.1016/j.palaeo.2007.10.032

Guntu RK, Rathinasamy M, Agarwal A, Sivakumar B (2020) Spatiotemporal variability of Indian rainfall using multiscale entropy. J Hydrol 587:124916. https://doi.org/10.1016/j.jhydrol.2020.124916

Guo A, Chang J, Wang Y, Huang Q, Guo Z (2017) Maximum entropy-copula method for hydrological risk analysis under uncertainty: a case study on the loess plateau. China Entropy 19(11):609. https://doi.org/10.3390/e19110609

IPCC Climate Change Synthesis Report (2014) Topic 2 future climate changes risks and impacts. Contribution of Working Groups I, II and III to the Fifth Assessment Report of the Intergovernmental Panel on Climate Change eds. Pachauri RK, Meyer LA (Geneva, Switzerland).

Jemai S, Ellouze M, Abida H (2017) Variability of precipitation in arid climates using the wavelet approach: case study of watershed of Gabes in South-East Tunisia. Atmosphere 8(9):178. https://doi.org/10.3390/atmos8090178

Jhong BC, Huang J, Tung CP (2019) Spatial assessment of climate risk for investigating climate adaptation strategies by evaluating spatial-temporal variability of extreme precipitation. Water Resour Manage 33:3377–3400. https://doi.org/10.1007/s11269-019-02306-8

Kayano MT, Andreoli RV (2006) Relationships between rainfall anomalies over northeastern Brazil and the El Niño-Southern Oscillation. J Geophys Res 111:D13101. https://doi.org/10.1029/2005JD006142

Kayano MT, Andreoli RV, De Souza RAF (2020) Pacific and Atlantic multidecadal variability relations to the El Niño events and their effects on the South American rainfall. Int J Climatol 40:2183–2200. https://doi.org/10.1002/joc.6326

Kendall MG (1948) Rank correlation methods. C. Griffin, London

Khan MI, Liu D, Fu Q, Azmat M, Luo M, Hu Y, Zhang Y, Abrar FM (2016) Precipitation variability assessment of northeast China: Songhua River basin. J Earth Syst Sci 125:957–968. https://doi.org/10.1007/s12040-016-0715-9

Krige DG (1966) Two-dimensional weighted moving average trend surfaces for ore-evaluation. J South Afr Inst Min Metall 66:13–38

Li Q, Yang M, Wan G, Wang X (2016) Spatial and temporal precipitation variability in the source region of the Yellow River. Environ Earth Sci 75(7):594. https://doi.org/10.1007/s12665-016-5583-8

Liang CP, Hsu WS, Wang CYC, SW, Chen JS, (2019) The combined use of groundwater quality, drawdown index and land use to establish a multi-purpose groundwater utilization plan. Water Resour Manage 33:4231–4247. https://doi.org/10.1007/s11269-019-02360-2

Liu J, Liu T, Bao A, De Maeyer P, Feng X, Miller SN, Chen X (2016) Assessment of different modelling studies on the spatial hydrological processes in an arid alpine catchment. Water Resour Manage 30(5):1757–1770. https://doi.org/10.1007/s11269-016-1249-2

Mann HB (1945) Nonparametric tests against trend. Econometrica: Journal of the econometric society, 245–259.

Marengo JA, Torres RR, Alves LM (2017) Drought in Northeast Brazil—past, present, and future. Theor Appl Climatol 129:1189–1200. https://doi.org/10.1007/s00704-016-1840-8

Maruyama T, Kawachi T, Singh VP (2005) Entropy-based assessment and clustering of potential water resources availability. J Hydrol 309(1–4):104–113. https://doi.org/10.1016/j.jhydrol.2004.11.020

Maurer EP, Lettenmaier DP, Mantua NJ (2004) Variability and potential sources of predictability of North American runoff. Water Resour Res 40:W09306. https://doi.org/10.1029/2003WR002789

Meshram SG, Singh VP, Meshram C (2017) Long-term trend and variability of precipitation in Chhattisgarh State. India Theor Appl Climatol 129(3):729–744. https://doi.org/10.1007/s00704-016-1804-z

Mishra AK, Singh VP (2010) A review of drought concepts. J Hydrol 391(1–2):202–216. https://doi.org/10.1016/j.jhydrol.2010.07.012

Mishra AK, Özger M, Singh VP (2009) An entropy-based investigation into the variability of precipitation. J Hydrol 370(1–4):139–154. https://doi.org/10.1016/j.jhydrol.2009.03.006

Qin FY, Jia GS, Yang J, Na YT, Hou MT (2018) Spatiotemporal variability of precipitation during 1961–2014 across the Mongolian Plateau. J Mt Sci 15(5):992–1005. https://doi.org/10.1007/s11629-018-4837-1

Ramarao MVS, Sanjay J, Mujumdar KR, M, Bazaz A, Revi A, (2019) On observed aridity changes over the semiarid regions of India in a warming climate. Theor Appl Climatol 136:693–702. https://doi.org/10.1007/s00704-018-2513-6

Roushangar K, Alizadeh F (2018) Entropy-based analysis and regionalization of annual precipitation variation in Iran during 1960–2010 using ensemble empirical mode decomposition. J Hydroinform 20(2):468–485. https://doi.org/10.2166/hydro.2018.037

Santos CACD, Brito JIBD, Rao TVR, Menezes HEA (2009) Tendências dos índices de precipitação no Estado do Ceará. Rev Bras De Meteorol 24(1):39–47. https://doi.org/10.1590/S0102-77862009000100004

Sen PK (1968) Estimates of the regression coefficient based on Kendall's tau. J Am Stat Assoc 63(324):1379–1389

Shannon CE (1948) A mathematical theory of communication. Bell Syst Tech 27(3):379–423

Singh VP (1997) The use of entropy in hydrology and water resources. Hydrol Process 11(6):587–626

Singh PK, Chudasama H (2021) Pathways for climate change adaptations in arid and semi-arid regions. J Clean Prod 284:124744. https://doi.org/10.1016/j.jclepro.2020.124744

Su HT, You GJY (2014) Developing an entropy-based model of spatial information estimation and its application in the design of precipitation gauge networks. J Hydrol 519:3316–3327. https://doi.org/10.1016/j.jhydrol.2014.10.022

Tongal H, Sivakumar B (2019) Entropy analysis for spatiotemporal variability of seasonal, low, and high streamflows. Stoch Environ Res Risk Assess 33(1):303–320. https://doi.org/10.1007/s00477-018-1615-0

Villalta DE, De Guenni LB, Sajo-Castelli AM (2020) Spatio-temporal modelling of hydro-meteorological derived risk using a Bayesian approach: a case study in Venezuela. Stoch Environ Res Risk Assess 34(3):513–529. https://doi.org/10.1007/s00477-020-01783-3

Wu Y, Liu S, Yan W, Xia J, Xiang W, Wang K, Luo Q, Fu W, Yuan W (2016) Climate change and consequences on the water cycle in the humid Xiangjiang River Basin. China Stoch Environ Res Risk Assess 30(1):225–235. https://doi.org/10.1007/s00477-015-1073-x

Yang H, Xiao H, Guo C, Sun Y (2019a) Spatial-temporal analysis of precipitation variability in Qinghai Province, China. Atmos Res 228:242–260. https://doi.org/10.1016/j.atmosres.2019.06.005

Yang X, Yang Y, Li K, Wu R (2019b) Estimation and characterization of annual precipitation based on spatiotemporal kriging in the Huanghuaihai basin of China during 1956–2016. Stoch Environ Res Risk Assess 34:1407–1420. https://doi.org/10.1007/s00477-019-01757-0

Zhang Q, Zheng Y, Singh VP, Xiao M, Liu L (2016) Entropy-based spatiotemporal patterns of precipitation regimes in the Huai River basin. China Int J Climatol 36(5):2335–2344. https://doi.org/10.1002/joc.4498

Zhang L, Li H, Liu D, Fu Q, Li M, Faiz MA, Khan MI, Li T (2019) Identification and application of the most suitable entropy model for precipitation complexity measurement. Atmos Res 221:88–97. https://doi.org/10.1016/j.atmosres.2019.02.002

Zheng Y, He Y, Chen X (2017) Spatiotemporal pattern of precipitation concentration and its possible causes in the Pearl River basin, China. J Clean Prod 161:1020–1031. https://doi.org/10.1016/j.jclepro.2017.06.156

Zhou F, Xu Y, Chen Y, Xu CY, Gao Y, Du J (2013) Hydrological response to urbanization at different spatio-temporal scales simulated by coupling of CLUE-S and the SWAT model in the Yangtze River Delta region. J Hydrol 485:113–125. https://doi.org/10.1016/j.jhydrol.2012.12.040